energy&fuels

pubs.acs.org/EF Article

Performance of Equilibrium FCC Catalysts in the Conversion of the SARA Fractions in VGO

Jayson Fals, Juan Rafael García, Marisa Falco, and Ulises Sedran*

Cite This: https://dx.doi.org/10.1021/acs.energyfuels.0c02804 Read Online

ACCESS | Metrics & More | Article Recommendations

ABSTRACT: Two equilibrium FCC catalysts of the octane-barrel (ECAT-D) and resid (ECAT-R) types were used in the cracking of a typical vacuum gasoil (VGO) and its saturated (SF), aromatic (AF), and resin (RF) fractions. The experiments were carried out in a batch, fluidized bed laboratory CREC Riser Simulator reactor. The reaction temperature was 500 °C, the catalyst-to-oil relationship was 1, with 0.2 g of the catalyst being used in each experiment, and the reaction times were 0.7, 1.5, and 3 s. The ranking of the reactivities of the different feedstocks was SF > VGO > AF > RF over both catalysts. While the AF and RF fractions yielded more gasoline than the SF fraction, the latter showed the highest yields of LPG. The coke forming trend followed the order SF < VGO < AF < RF. Even though catalyst ECAT-D, with a higher and stronger acidity, was more active than catalyst ECAT-R, which has less acidity and better textural properties (higher mesoporosity and pore diameter), the latter was less affected by coke deposition, considering the changes in the specific surface area and acidic properties after use. Coke impacted more severely on Brönsted acid sites than on Lewis sites, particularly when the AF and RF fractions were used. The stronger acid sites were more severely affected by coke, particularly in catalyst ECAT-D. The negative effect on strong acidic sites was consistent with the increasing basic character of the feedstocks, following the order SF < VGO < AF < RF.

1. INTRODUCTION

Among the conversion processes in refineries, the catalytic cracking of hydrocarbons in fluidized beds (fluid catalytic cracking, FCC) is considered one of the most profitable and versatile.[1−3] FCC units process heavy feedstocks, mainly gas oils from vacuum distillation (VGO) but also mixtures of VGO and residues from atmospheric distillation and/or other heavy cuts from thermal conversion processes, to get lighter and much more valuable hydrocarbons.[4−6] Among the FCC products, gasoline and middle distillates are used in the production of transportation fuels, while the light olefins are useful for petrochemical raw materials, with the demand for propylene increasing notoriously in recent years.[7] After its initial development, FCC has undergone a large number of modifications and improvements in terms of both hardware and catalyst technology, making it possible to increase its efficiency and benefits and meet the specific demands of each refinery.[8−11]

A detailed characterization of the properties of a given feedstock is of great importance to establish optimal strategies and process conditions. Typical FCC feedstocks are complex hydrocarbon mixtures, which are constituted by two main groups: maltenes and asphaltenes. Maltenes include molecules with aromatic, naphthenic, and paraffinic structures, which are soluble in saturated hydrocarbons with a low boiling point. Asphaltenes comprise molecules with condensed aromatic rings and a high content of heteroatoms and metals.[12−15] A high proportion of heteroatoms such as sulfur and nitrogen in the feedstocks impose the use of hydrotreating processes in order to meet the standards of quality of the products.[16] Moreover, the negative effect of nickel, vanadium, and iron contaminating metals on the activity, selectivity, and stability of the FCC catalysts has been widely reported.[17,18]

According to their solubility in different solvents with increasing polarity, four fractions can be distinguished in a VGO: saturated, aromatic, resin, and asphaltenes, thus defining its SARA composition.[19] Given the different natures of the molecules that constitute each fraction, different behaviors can be expected for them in the FCC process, i.e., different reactivities, product selectivities, and coke yields.[20]

In order to know the SARA composition of a heavy cut of hydrocarbons, fractionation based on the solubility of the individual fractions in specific organic solvents can be performed as described in the ASTM D2007−11 standard.[19] The method allows for separating saturated hydrocarbons (SF, nonpolar compounds including linear, branched, and cyclic hydrocarbons);[21] aromatic hydrocarbons (AF, more polar compounds, with aromatic rings); resin hydrocarbons (RF, with molecules having highly polar, condensed polyaromatic structures, associated with the stabilization of asphaltenes);[22,23] and asphaltene hydrocarbons (AsF, complex structures with condensed polyaromatic rings, short aliphatic side chains, and a higher proportion of heteroatoms such as nitrogen, oxygen, sulfur, and metals). The AsF fraction exists in minor

Received: August 18, 2020
Revised: October 23, 2020

Downloaded via CONICET on November 25, 2020 at 12:02:06 (UTC).
See https://pubs.acs.org/sharingguidelines for options on how to legitimately share published articles.

ACS Publications © XXXX American Chemical Society

proportions in typical FCC feedstocks, constituting the most polar fraction, which is in part responsible for the high viscosity of heavy cuts.

In addition to the complete characterization of the feedstock, it is essential to characterize and evaluate the catalysts to be used in the process. FCC catalysts are compounds, with Y zeolite being their most important component (15−40 wt %), which is deposited on an active or inert matrix together with specific additives that depend on many operation and commercial target issues.[11,24−28] Considering the specific process conditions and the nature of the feedstock, the catalyst should meet a number of requirements, such as thermal and hydrothermal resistance, tolerance toward metal poisoning (especially, Ni and V), appropriated coke yield, and low resistance to intraparticle mass transfer,[29] in order to achieve the desired performance. Thus, tailor-made catalysts are formulated for the FCC process. In this sense, octane-barrel type catalysts were developed to maximize the yield of gasoline and its quality (RON number) in a balanced result. On the contrary, specific catalysts for processing resids should ensure an appropriated accessibility of bulky molecules to the acidic sites,[24,30,31] as well as a good thermal stability and a high resistance to contaminant species, which are particularly present in those feedstocks.[26−29]

Given the carbocationic mechanisms governing the complex set of reactions in the FCC process, the performance of a given catalyst is strongly constrained by its acidic properties.[32] Then, both the activity and selectivity toward different products will depend on the density, nature (Brönsted or Lewis), and strength of the acid sites.[33] Besides acidity, the catalyst textural properties also play an important role in the observed activity and selectivity, as well as in catalyst deactivation.[32]

The operation regime of a FCC unit is affected by the deactivation of the catalyst due to coke deposition, which negatively affects the acidic and textural properties.[9,20] Both the amount of coke on the catalyst and its nature depend on the feedstock composition, catalyst properties, and reaction conditions.[20,34] Thus, it is important to understand and, hopefully, predict the impact of processing feedstocks with different natures on the coke deposition and, consequently, on catalyst deactivation and unit operation. Given the need to improve the overall efficiency of the process, catalyst deactivation by coke plays an important role, which has been the subject of multiple investigations.[33−37]

In general, the individual reactivities of the SARA fractions occurring in the different streams fed into the FCC process; their specific contributions to the various products and their effects on the catalyst deactivation are poorly known. It is the objective of this work to evaluate the impact of the properties of two equilibrium FCC catalysts (an octane-barrel type catalyst and a resid catalyst) over their activities and selectivities in the cracking of SARA fractions in a VGO as compared to the parent feedstock under conditions similar to those in commercial units. The specific contribution of each fraction on the coke yield and nature, as well as its effect on the variation of the acidic and textural properties of both catalysts, are also studied.

2. EXPERIMENTAL SECTION

2.1. VGO and SARA Fractions. A vacuum gasoil (VGO) and three of its constituent fractions (saturated fraction (SF), aromatic fraction (AF), and resin fraction (RF)) were used as feedstocks. The main properties of the VGO are shown in Table 1.

Table 1. Feedstock Properties

degree API	23
aniline point (°C)	80.1
CCR (wt %)[a]	0.11
distillation curve (°C)[b]	
initial	199
10 vol %	345
50 vol %	438
90 vol %	495
final	512
SARA fractions (wt %)[c]	
saturated (SF)	68.12
aromatic (AF)	19.90
resin (RF)	10.31
asphaltene (AsF)	0.81
nickel (ppm)	0.10
vanadium (ppm)	0.73

[a]ASTM D-4530. [b]ASTM D-1160. [c]ASTM D-2007.

The saturated, aromatic, resin, and asphaltene (SARA) fractions were separated from the VGO following the procedure described in the ASTM D2007−11 standard. First, the asphaltenes were separated by precipitation using *n*-pentane, leaving the fraction of maltenes in solution. Then, the solubilized saturated, aromatic, and resin fractions were separated by means of two in-series chromatographic columns: the upper one was packed with Attapulgus clay, which selectively adsorbs polar compounds (resins), while the bottom column was packed with silica gel, which selectively adsorbs aromatic compounds. Once the maltene fraction was fed on the top of the upper column, *n*-pentane was passed through the columns in order to remove the saturated compounds. Then, the columns were disassembled and the top column was swept with a 50:50 acetone/toluene mixture to remove the resins, with the bottom column being swept with toluene to remove the aromatic compounds. Finally, the solvent was removed from each fraction in a rotating evaporator.

The elemental composition (Ni and V content) was determined by inductively coupled plasma optical emission spectroscopy (ICP-OES). A previously weighed sample was burnt in an air stream. The ashes were treated with hydrofluoric acid in a Milestone START D microwave digester. They were then brought to a known volume using deionized water and filtered. The final solution was analyzed by argon-induced plasma atomic emission spectroscopy on a PerkinElmer ICP OPTIMA 2100 spectrometer.

2.2. Catalyst Evaluation Tests. The experiments of catalytic cracking were performed in a CREC Riser Simulator reactor, which was specifically designed to closely mimic the conditions of the commercial FCC process.[8] Two equilibrated commercial FCC catalysts were used: ECAT-D and ECAT-R were octane-barrel and resid type catalysts, respectively. An octane-barrel catalyst, aimed at achieving a high gasoline yield and quality, is characterized by a moderated content of Y zeolite, with a low content of rare earth elements and a relatively low unit cell size.[38] A resid type catalyst, formulated to face residual fractions, has a lower content of crystalline material, with a higher content of rare earths (responsible of a higher hydrothermal stability), a better accessibility of bulky molecules to the acidic sites, and a high resistance to contaminant metals.[29,39,40] Both ECAT-D and ECAT-R catalysts were used as received from the corresponding refineries. After loading them in the reactor and before the experiments, they were regenerated under an air stream at 570 °C during 30 min. The reaction temperature was 500 °C, the catalyst-to-oil relationship was 1, with 0.2 g of catalyst being used in each experiment, and the reaction times were 0.7, 1.5, and 3 s. These conditions ensure the proper contact of the fluidized catalyst bed with reactants.[8,41] The products were analyzed online in a Varian 450 GC chromatograph using a nonpolar, dimethylpolysiloxane column (30 m long, 250 μm diameter, and 0.25 μm film thickness) and a flame ionization detector. Conversion was defined as the sum of the mass

https://dx.doi.org/10.1021/acs.energyfuels.0c02804
Energy Fuels XXXX, XXX, XXX−XXX

yields of dry gas (DG, C_1−C_2), liquefied petroleum gas (LPG, C_3−C_4), gasoline (C_5-216 °C), light cycle oil (LCO, 216−343 °C), and coke fractions. The mass balances (recoveries) were close to more than 90 wt % in all the experiments. The research octane numbers of the gasoline cuts were calculated following the method by Anderson.[42]

The yield of coke was determined by means of temperature-programmed oxidation (TPO) experiments. After the experiments in the Riser Simulator reactor, once the reaction time is achieved and products are evacuated, the catalyst is flushed with a N_2 stream during 15 min at the reaction temperature. Twenty milligrams of coked catalyst particles were heated at 250 °C by passing a N_2 flow of 50 cm^3/min during 30 min at 250 °C. Then, the flow was switched to a O_2 (1%)/N_2 (balance) stream at 12 °C/min up to 700 °C. The carbon oxides formed during coke combustion were then converted into methane by circulating the effluent gas stream over a Ni catalyst at 400 °C, and the amount of methane was quantified with the aid of a flame ionization detector in a Shimadzu GC-8A gas chromatograph.

2.3. Catalyst Characterization. The catalysts were characterized before and after the experiments of catalytic cracking. The textural properties were determined using a Micromeritics ASAP 2020 sorptometer. The specific surface areas were calculated by means of the Brunauer−Emmet−Teller (BET) model. The total pore volumes were evaluated from the amount of nitrogen adsorbed up to P/Po ∼ 0.98. The mesopore size distributions and mean pore diameters were obtained from the Barrett−Joyner−Halenda (BJH) method. The mesopore surface areas and micropore volumes were calculated using the *t*-plot method. The zeolite content was estimated from the micropore specific surface area by using the correlation proposed by Johnson.[43]

The acidic properties (nature, strength, and density of acid sites) of both fresh and coked catalysts were evaluated by means of Fourier transform infrared (FTIR) spectroscopy and temperature programed desorption (TPD) experiments using pyridine as a test molecule in both cases. The FTIR analyses were performed in a Shimadzu FTIR Prestige-21 spectrophotometer. Approximately 100 mg of each sample was pressed at 1 ton/cm^2 to conform self-supported 2.3 cm^2 wafers that were then placed into a cell with CaF_2 windows. The samples were initially degassed during 2 h at 450 °C and 10^{-4} Torr, and a background spectrum was collected after cooling down at room temperature. The adsorption of pyridine (Merck, 99.5 wt %) was performed at room temperature, and the corresponding spectra were recorded in the range 1700−1400 cm^{-1} with a resolution of 4 cm^{-1} after successive desorptions (150, 300, and 400 °C). The amount of Brönsted and Lewis acid sites were calculated from the integrated absorbance of the bands at 1545 and 1450−1460 cm^{-1}, respectively, and their corresponding integrated molar extinction coefficients.[44] In the case of the coked catalysts, the background FTIR spectra allowed us to study the nature of coke formed over each catalyst. In this sense, the signal at 1580 cm^{-1} was attributed to "aromatic type" coke while the signal at 1610 cm^{-1} was associated with "olefinic type" coke.[45,46]

The TPD of pyridine was used in order to determine the density and strength of the acid sites. The adsorption of pyridine over the catalysts was performed by means of a stream of N_2 saturated with pyridine at 80 °C. The physically adsorbed pyridine was removed by being flushed with N_2 at 150 °C during 1 h. Then, the sample was heated from 150 to 800 °C following a heating ramp of 12 °C/min. The desorbed pyridine was detected and quantified after methanation with the aid of a flame ionization detector.

3. RESULTS AND DISCUSSION

3.1. SARA Fractioning and Feedstock Characterization. The main properties of the parent VGO, which can be considered paraffinic in nature, are shown in Table 1. According to its API gravity of 23°, this feedstock is defined as a medium oil.[47] This density can be related to the high content of linear paraffinic hydrocarbons. Moreover, the low CCR index (0.11 wt %), which is an indicator of the coke forming potential during conversion processes, is consistent with the API density.[48,49] The simulated distillation curve of VGO, which showed that 10% of the components are distilled at 345 °C and 90% at 495 °C, is also in agreement with the API density.

The parent VGO was fractionated into its SARA fractions with high efficiency, as indicated by the 99.14 wt % recovery of the initial VGO mass (see Table 1). As it can be seen in Table 1, the paraffinic nature of the VGO was confirmed by the important proportion of the saturated fraction (SF), which amounted to 68.12 wt %. The following most abundant fractions were aromatic (AF) and resin (RF) fractions, with their yields being 19.90 and 10.31 wt %, respectively. The asphalthene fraction (AsF) represented only 0.81 wt % of the VGO. The GC analysis showed that molecules in the range from 12 to 40 carbon atoms per molecule were predominant in the most important fractions SF and AF, with *n*-paraffins being major in the saturated fraction.

The separation of complex hydrocarbon feedstocks, such as VGO or atmospheric tower residues (ATR), showed to be useful not only to determine the characteristics of a given feedstock but also, allegedly, to predict performances under commercial operations.[50] Under this concept, Xu et al.[1] correlated the SARA compositions of various FCC feedstocks with the product yields, for example, the aromatic fraction favored the yield of gasoline, while the resin fraction favored the yield of coke. Similar results were reported by Nilsson and Otterstedt,[51] who studied this issue in the catalytic cracking of heavy vacuum gas oils, showing that fractions with a highly polar character increased the yield of aromatic gasoline with higher RON values.

The prediction of reactivity and product distribution to be observed in a FCC unit of a given feedstock used, based on its composition, was also attempted by means of kinetic models.[52] However, it was shown that it is not possible to faithfully extrapolate the results to the commercial process due to the very complex and singular properties of the hydrocarbon cuts. Indeed, the catalyst selection methods do include simulations based on empirical models that also incorporate laboratory experimental information obtained from different reactor configurations, which, in most of the cases, can not reproduce the commercial conditions.[53]

3.2. Catalyst Properties. The most important properties of the commercial equilibrium FCC catalysts used in this work are shown in Tables 2 and 3. It should be taken into account

Table 2. Catalysts Properties

	ECAT-D	ECAT-R
BET specific surface area (m^2/g)	152	123
micropore specific surface area (m^2/g)[a]	122	82
total pore volume (cm^3/g)	0.102	0.128
mesopore volume (cm^3/g)[a]	0.056	0.079
average mesopore diameter (Å)	110	122
zeolite content (wt %)[b]	16.9	14.8
rare earth oxides content (wt %)	1.26	2.94
unit cell size (Å)[c]	24.23	24.27
Fe (ppm)	2800	4200
Ni (ppm)	4000	5100
V (ppm)	2700	5800

[a]Micropore specific surface area = BET specific surface area − mesopore specific surface area. Mesopore volume = total pore volume − micropore volume. [b]Johnson's method.[43] [c]ASTM D3942−85.

https://dx.doi.org/10.1021/acs.energyfuels.0c02804
Energy Fuels XXXX, XXX, XXX−XXX

Table 3. Concentration of Brönsted (B) and Lewis (L) Acid Sites (μmol Py/g) from FTIR Experiments in Catalysts ECAT-D and ECAT-R

	ECAT-D		ECAT-R	
T_{des} (°C)	Brönsted	Lewis	Brönsted	Lewis
150	11.9	13.5	8.0	4.2
300	9.7	10.4	6.2	3.6
450	8.2	9.0	4.1	2.2

that these commercial catalysts are equilibrated, that is, they are actual catalysts operating in refineries, with their properties being average for the whole inventory and particles having a wide age distribution.[54]

As expected, the properties differ significantly between catalysts, given that they were formulated according to markedly different operation objectives. The most important differences in the textural properties in catalyst ECAT-R (lower specific surface area and micropore contribution and higher mesopore diameter and mesopore volume) as compared to those in catalyst ECAT-D support in part their expected performances. In effect, catalyst ECAT-R was designed to process feedstocks with a certain proportion of resids, which includes molecules with a larger molecular size, facing more severe diffusion restrictions in the catalyst pore system. In this sense, a higher contribution to the pore volume from mesopores with a larger size, as confirmed by the BJH method, can be particularly appropriated. The impact of the FCC catalyst textural properties on their catalytic performance has been extensively discussed.[20,30,31,55−61]

The different operational environments imposed on the two catalysts are reflected on the different contents of the contaminant metals. In effect, catalyst ECAT-R has higher contents of Fe, Ni, and V, thus evidencing its contact with resid feedstocks, which include higher proportions of metal containing hydrocarbons than conventional, lighter feedstocks.[16]

An inspection by XRD confirmed that the only zeolite solid found in both catalysts was Y zeolite. The lower unit cell size and content of rare earth elements that provide a higher hydrothermal resistance to FCC catalysts[39,40] in catalyst ECAT-D, as compared to those in catalyst ECAT-R, are typical in octane-barrel catalysts, where both the gasoline yield and quality (RON) are expected to be maximized.[38]

The results of acidity characterization are shown in Table 3 and Figure 1. It can be seen that the total acidity in catalyst ECAT-D, as given by the amount of pyridine remaining adsorbed after desorption at 150 °C, was significantly higher than that in catalyst ECAT-R. This is also true if each of the different types of acid sites or desorption temperatures are considered. This should be understood as the final balance between the factors impacting oppositely on catalyst acidity. If the zeolite topology is the same, Y zeolite in this case, the greater the amount of zeolite with a given UCS, the higher the acidity; on the contrary, if the zeolite content was the same, the smaller the content of REO and the UCS, the lower the acidity.

The pyridine TPD analysis showed that strong acidic sites prevail in both catalysts, independent of the site type. In effect, the TPD profiles exhibited two peaks (refer to Figure 1), the first one corresponding to pyridine desorbed at a low temperature (340−360 °C), assigned to weak acid sites, and the second one peaking at about 600 °C, assigned to strong acid sites. In the case of catalyst ECAT-D, the area fractions of

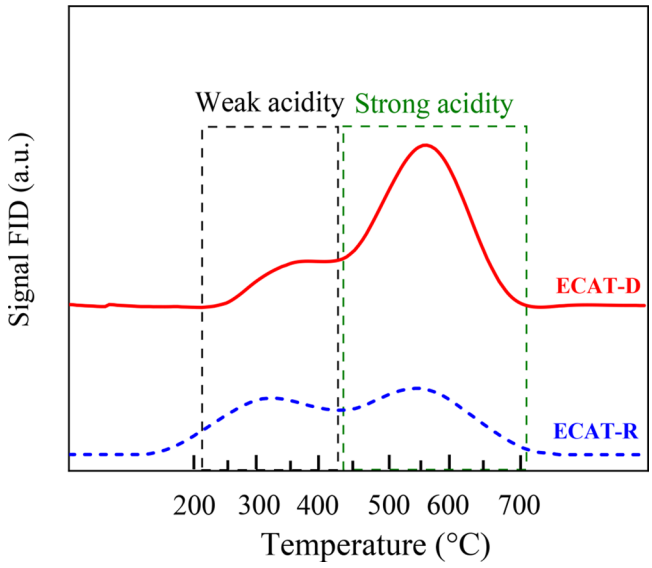

Figure 1. Pyridine TPD profiles of ECAT-D and ECAT-R catalysts.

the first and second peak were 25 and 75%, respectively, while those in the case of ECAT-R were 42 and 58%.

3.3. Catalytic Performance. *3.3.1. Conversion.* The catalytic performance of the two equilibrium commercial catalysts was evaluated in the conversion of the parent VGO and, individually, of its most important constitutive fractions (saturated SF, aromatic AF, and resin RF). The reaction temperature (500 °C) was typical of the commercial FCC process, but the other conditions, particularly reaction times and catalyst-to-oil relationship, were chosen to avoid excessive coke yields, which could impact severely on the physical (textural) and chemical (acidic) properties of the catalysts and mask some changes and evidence. In this sense, the fluidized bed in the CREC Riser Simulator reactor allows for a more efficient catalyst−reactants contact, thus avoiding the high coke yields observed in fixed bed reactors.[8,38]

Figure 2 shows the conversions of all the feedstocks on the equilibrium catalysts as a function of reaction time. Even

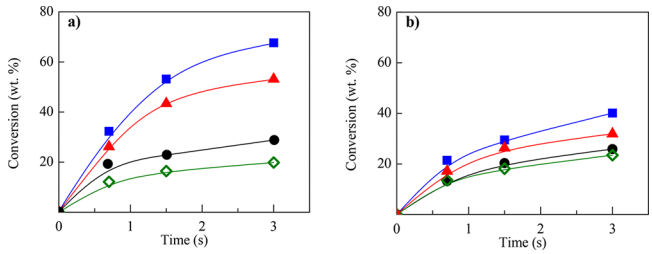

Figure 2. Conversion of the various feedstocks at 500 °C over (a) catalyst ECAT-D and (b) catalyst ECAT-R. Symbols: triangles, VGO; squares, SF; circles, AF; open diamonds, RF.

though the absolute values of conversion do not match those found in the commercial operation,[4] given the operating conditions chosen for these experiments, distinctive behaviors can be observed. It can be seen from the conversion profile of the commercial feedstock VGO that catalyst ECAT-D is more active than catalyst ECAT-R. The conversion of the resin fraction (RF), which is a polar fraction, including bulkier molecules, was slightly higher over catalyst ECAT-R. In this sense, the higher accessibility provided by this catalyst can

https://dx.doi.org/10.1021/acs.energyfuels.0c02804
Energy Fuels XXXX, XXX, XXX−XXX

Table 4. Distributions of Products (selectivities, wt %) in the Conversion of the Various Feedstocks[a]

	ECAT-D				ECAT-R			
	VGO	SF	AF	RF	VGO	SF	AF	RF
S_{DG}	5.8	9.7	4.4	6.1	3.9	5.3	5.0	10.8
S_{LPG}	6.3	12.4	5.2	6.7	4.8	16.2	5.1	12.0
$S_{gasoline}$	25.9	26.0	32.2	34.8	22.1	20.1	27.3	28.8
S_{LCO}	59.9	51.0	54.8	46.4	67.3	57.4	60.5	44.9
S_{coke}	2.0	0.9	3.4	6.0	1.8	1.0	2.1	3.5

[a]Conversion approximately 20 wt %.

Table 5. Composition of the Gasoline Cut (wt %) in the Conversion of the Various Feedstocks[a]

	ECAT-D				ECAT-R			
	VGO	SF	AF	RF	VGO	SF	AF	RF
paraffins	28.6	31.8	14.7	10.5	30.5	35.5	14.4	12.3
olefins	25.2	29.1	11.1	10.9	23.1	26.3	22.9	16.8
naphthenes	17.1	15.1	12.2	11.4	18.3	17.1	9.6	11.1
aromatics	29.1	24.0	62.0	67.2	28.1	21.1	53.1	59.8
RON	80	79	83	84	77	76	82	83

[a]Conversion approximately 20 wt %.

contribute positively to a more extensive cracking of that feedstock. These observations can be rationalized in view of the commercial global definitions of the octane-barrel (ECAT-D) and resid (ECAT-R) catalysts. In effect, the higher zeolite content and acidity in catalyst ECAT-D provide a higher activity and gasoline yield, as well as its lower UCS would provide a higher fuel quality in the products (see Section 3.3.2). Catalyst ECAT-R, designed for processing residual fractions, is clearly less active, as shown by the conversion profiles of VGO and the SF and AF fractions; the selectively slightly higher conversion of fraction RF could be justified on the basis of the higher proportion of mesopores, which, as previously discussed, would facilitate the diffusion transport of bulky molecules as those present among resins.

The order of reactivity of the different fractions was SF > VGO > AF > RF over both catalysts. It is to be noted that the conversion of the parent feedstock cannot be reconstructed following an additive approach starting from the conversion of the individual fractions composing it. This fact has been observed in a previous work with the fractions composing an atmospheric tower resid converting on a resid catalyst, which was attributed to the existence of interactions between the individual components of the fractions when present in the parent mixture.[29]

3.3.2. Product Distributions. The distributions of the products in the conversion of the various feedstocks are shown in Table 4 in the form of selectivities observed at about 20 wt % conversion. The selectivities were calculated as the relationship between the yield of the corresponding hydrocarbon cut and the conversion of the feedstock injected in each experiment. These selectivities cannot be compared to usual commercial values, given the experimental conditions, but allow for comparisons between feedstocks and catalysts. It can be seen that in all the cases LCO is the major product, followed by gasoline, LPG, and DG. This ranking is consistent with the experimental conditions and the consequent degree of extension of the reactions.

It was observed over both catalysts that the aromatic (AF) and resin (RF) fractions yield significantly more gasoline than the saturated (SF) fraction, which, in turn, shows the highest yield of LPG. The hydrocarbons composing AF and RF fractions possess base structures that have common features, being mainly constituted by condensed aromatic rings with side chains that could be easily dealkylated, thus originating new aliphatic and aromatic hydrocarbons in the gasoline boiling range.[1,49,50] The catalytic cracking of the SF, AF, and RF fractions obtained from an ATR showed similar results.[29] Clearly, again the yields from the individual fractions cannot be used to estimate the yield of a given group when the parent VGO is cracked, that is, they are not directly additive.

When VGO and its main constituting fraction (SF) were cracked, the most active catalyst, ECAT-D, yielded more light products than catalyst ECAT-R. It can be seen in relation to coke that catalyst ECAT-D, consistently with its higher acidity, yields more coke than catalyst ECAT-R, with the differences being more important in the cases of the more complex fractions AF and RF, where the concentrations of coke precursors are higher. Moreover, the coke forming trend of the fractions is, as expected over both catalysts, RF > AF > SF. A more detailed analysis on the nature of the different cokes is presented in Section 3.3.3.

The distribution of hydrocarbons in the gasoline boiling range is shown in Table 5. It can be seen that, as justified previously according to their compositions,[1,49−51] aromatic AF and resin RF fractions produce much more aromatic compounds than the other fractions. The saturated SF fraction showed the highest contribution to paraffinic and olefinic hydrocarbons in the range, as expected from the direct cracking of the linear paraffins in that particular fraction feedstock. Moreover, independently from the catalyst, it can be seen that the behavior of the parent VGO feedstock was similar to that of the saturated fraction, given its predominance (see Table 1). The expected superior performance of catalyst ECAT-D (an octane-barrel catalyst) in terms of gasoline quality is also evident, which, for a given feedstock, is always higher than that of the gasoline produced by catalyst ECAT-R.

3.3.3. Coke Yield and Characteristics. Figure 3 shows the yields of coke as a function of reaction time in the cracking of the various feedstocks. It can be observed that each of the feedstocks produced more coke on catalyst ECAT-D than on

https://dx.doi.org/10.1021/acs.energyfuels.0c02804
Energy Fuels XXXX, XXX, XXX−XXX

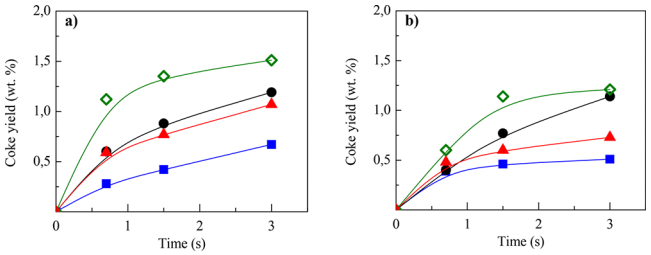

Figure 3. Coke yields from the various feedstocks at 500 °C over (a) catalyst ECAT-D and (b) catalyst ECAT-R. Symbols: triangles, VGO; squares, SF; circles, AF; open diamonds, RF.

catalyst ECAT-R, given that ECAT-D is more active, as the consequence of having a higher acidity and stronger acid strength. In the case of catalyst ECAT-R, besides its less acidic character, the higher mesoporosity could also contribute to form less coke by increasing the diffusion of coke precursors out of the pore system.

It is generally accepted that the importance as coke precursors of the hydrocarbon types occurring in a FCC feedstock is the following: alkenes < dienes < aromatics < polyaromatics. Most of the coke should be formed on the zeolite component, but, depending on the catalyst type, the matrix could also form coke.[35−37] The fractions RF and AF clearly produced more coke over both catalysts than fraction SF, with the VGO showing an intermediate yield. The higher coke yields from the fractions RF and AF are justified on their compositions, which includes coke precursors with a high molecular weight and basicity, which is consistent with a strong adsorption on the acidic sites favoring the reactions leading to coke.[12,13] These results are in line with observations from Pujro et al.[29] in the cracking of the SAR fractions from an ATR resid.

Figure 4 shows examples of the TPO profiles of the coke deposits formed from saturated (SF) and resin (RF) fractions

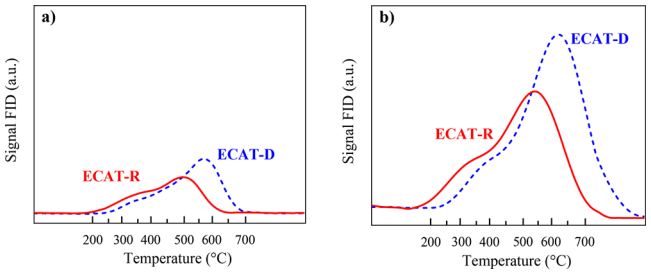

Figure 4. Combustion profiles of the coke deposits on catalysts ECAT-R (full lines) and ECAT-D (dashed lines) at 500 °C. Feedstocks: (a) saturated fraction, SF and (b) resin fraction, RF. Conversion at approximately 20 wt %.

on the equilibrium catalysts. Two combustion peaks can be observed in most of the cases located at, qualitatively, low and high temperatures. For the other feedstocks, VGO and AF, those two peaks were observed too (figures not shown). It is widely accepted that low temperature TPO peaks in the range 200−400 °C correspond to the combustion of a poorly developed coke with a relatively high H/C ratio. High temperature TPO peaks above 500 °C indicate the combustion of highly developed coke with condensed aromatic and diene-type structures with lower H/C relationships.[37] Differences can be observed between the catalysts. For example, the low temperature peak in the case of catalyst ECAT-D is located at 350−400 °C approximately, while that for catalyst ECAT-R is located at 300 °C approximately; the high temperature peaks are located at temperatures in the ranges 570−630 and 480−530 °C, respectively. These differences suggest that, for every feedstock, coke formed on the octane-barrel catalyst (ECAT-D) is, at least, more condensed than coke formed by the resid catalyst (ECAT-R). Note that the conversion achieved in all the cases is approximately the same; then, a higher extension of the set of cracking reactions could not be considered the reason for these differences in coke quality. Indeed the higher acid strength in catalyst ECAT-D could justify a stronger adsorption of coke intermediates and coke itself. As a consequence, this particular type of coke would require more energy to be burnt off. On the contrary, weaker adsorption processes would prevail on catalyst ECAT-R.

The increasing order of peak temperatures among the different feedstocks was VGO ≈ SF < AF < RF. The same ranking was previously observed during the cracking of VGO and its constitutive fractions over zeolites with different intracrystalline mesoporosities.[20] This confirms that the resin fraction RF is the one producing the most condensed coke (low temperature peak at about 400 °C and high temperature peak at about 630 °C, over catalyst ECAT-D), consistently with its higher proportion of polyaromatic molecules with a high basicity, which tend to be adsorbed more strongly on acidic catalytic sites.

More details on the nature of the coke, which may indicate differences from the various feedstock sources, can be observed in the FTIR spectra of the catalysts' surfaces after reaction. Two different main characteristic bands were observed: one at 1580 cm^{-1}, which can be assigned to "aromatic type" coke, showing the vibrations of condensed aromatic rings, and another one at 1610 cm^{-1}, assigned to "olefinic type" coke, showing the vibration of compounds with conjugated double bonds.[20,37,45,46] Both bands were observed in the coked catalysts ECAT-D and ECAT-R after the conversion of all the feedstocks (figures not shown), with differences being observed only in the intensity of the signals. Table 6 shows the intensities of the FTIR bands at 1580 and 1610 cm^{-1} observed from the catalyst surfaces after the conversion of the various feedstocks. Different from the saturated fraction SF,

Table 6. Relative Intensities of the FTIR Bands Assigned to Aromatic Coke (1580 cm^{-1}) and Olefinic Coke (1610 cm^{-1}) Formed during the Conversion of the Various Feedstocks at 500 °C[a]

	ECAT-D				ECAT-R			
	VGO	SF	AF	RF	VGO	SF	AF	RF
aromatic band (1580 cm^{-1})	1.00	0.71	2.92	5.22	0.74	0.47	2.20	3.60
olefinic band (1610 cm^{-1})	0.69	0.39	1.33	3.31	0.89	0.72	2.07	2.78

[a]Conversion approximately 20 wt %.

https://dx.doi.org/10.1021/acs.energyfuels.0c02804
Energy Fuels XXXX, XXX, XXX−XXX

which mainly includes nonpolar compounds such as linear, branched, and cyclic hydrocarbons, both aromatic AF and resin RF fractions include hydrocarbons with high polarity and condensed aromatic structures.[12,15] In the case of the resid catalyst ECAT-R, a marked aromatic character was observed in the coke formed only when AF and RF fractions were cracked (refer to Table 6), a fact that can be attributed to the nature of the species predominating in those fractions. Even though this catalyst (ECAT-R) is less acidic and its sites are weaker, its larger mesopore volume could allow it to host bulky aromatic molecules,[20] predominantly in AF and RF fractions, which are precursors of carbonaceous deposits with a high aromatic character. On the contrary, when catalyst ECAT-D was used, the type of coke prevailing was the aromatic one in all cases, including when VGO and saturated fraction (SF) were used as feedstocks. This behavior in the performance of catalyst ECAT-D could be attributed to the effect of higher acid site density (see Table 3), which favors condensation reactions leading to a higher aromatic character.

3.3.4. Changes in Catalyst Textural Properties. Figure 5 shows the changes in the textural properties of the equilibrium

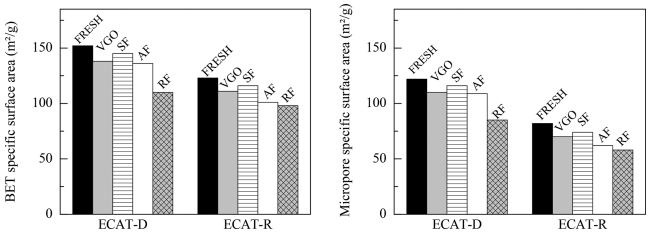

Figure 5. Textural properties of the fresh and coked catalysts used in the cracking of the various feedstocks. Conversion approximately 20 wt %.

catalysts after cracking of the various feedstocks at similar conversions, as compared to those of the fresh catalysts. As expected, the textural properties of both catalysts were affected by the deposition of coke during the cracking of the different feedstocks. The order in which the different feedstocks impacted the specific surface area was SF < VGO < AF < RF. It is clear that this order is coincident with the trend to form coke (coke yield) of each feedstock (see Figure 3). The losses in the BET specific surface area of catalyst ECAT-D during the reaction were up to 30%, while those in the case of ECAT-R were up to 20%. The micropore specific surface area, which is contributed by the zeolitic component in FCC catalysts, suffered losses in the same order when the different feedstocks where cracked (SF < VGO < AF < RF), with losses up to 30% in both catalysts. Besides the losses in the specific surface area, reductions in the mean mesopore diameters were also observed. Once again, the order in which the different feedstocks affected both catalysts was SF < VGO < AF < RF, with catalyst ECAT-D being the most affected.

3.3.5. Changes in Catalyst Acidic Properties. Table 7 shows the amount of total acidity in the catalysts before and after the conversion of each of the feedstocks (approximately 20 wt % in all cases). The yields of coke are shown between brackets. Clearly, the higher the yield of coke, the more severe the losses in acidity. Similarly to the case of the changes in textural properties, the order in which the different feedstocks produced losses of acidity was SF < VGO < AF < RF. The comparison between the catalysts shows that the relative losses of acidity in catalyst ECAT-R were lower than those observed in catalyst ECAT-D. For example, the conversion of the saturated fraction on catalyst ECAT-D caused a loss of about 38% of acidity, while it was only 29% on catalyst ECAT-R, even though the coke on the catalyst was higher in the case of ECAT-R (0.39 wt %, in comparison to 0.28 wt % over ECAT-D). As is shown in Table 6, the coke with aromatic character had greater predominance over the octane-barrel type catalyst ECAT-D when compared with that over the resid catalyst ECAT-R.

The same changes in acidity are shown normalized considering the coke yields (see Figure 6). It can be seen

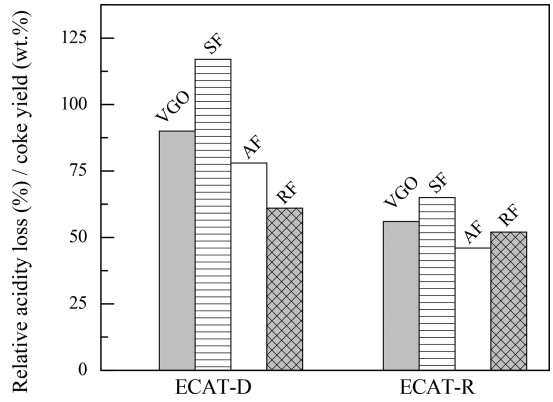

Figure 6. Normalized losses of acidity in the catalysts after the conversion of the various feedstocks at 500 °C. Conversion at approximately 20 wt %.

that the saturated fraction SF produced the coke with the highest negative effect per mass unit of coke produced, followed by the VGO. This characteristic, which had been previously observed in the cracking of VGO and its SARA fractions over Y zeolites with different degrees of intracrystalline mesoporosity,[20] could be attributed to the fact that the molecules comprising the SF fraction may access the acidic sites in the catalysts more easily, as compared to the hydrocarbons in the other fractions, which are bulkier. Then, the coke formed from the saturated fraction (SF) covers a higher proportion of acidic sites in the inner surface area of the catalysts. It could be expected that the coke formed from the aromatic AF and resin RF fractions would deposit more preferentially on the external surface area of the zeolite crystals or the matrix, given the more restricted accessibility of their molecules to the inner acidic sites of the zeolite.[62] The comparison between the catalysts shows that the losses of

Table 7. Total Acidity (μmol Py/g) in Fresh and Coked Catalyst after the Conversion of the Various Feedstocks at 500 °C[a]

	fresh	VGO	SF	AF	RF
ECAT-D	25.4	11.2 (0.59)	15.8 (0.28)	6.6 (0.88)	3.6 (1.51)
ECAT-R	12.2	6.1 (0.48)	8.7 (0.39)	5.0 (0.40)	4.1 (0.60)

[a]Conversion approximately 20 wt %. Coke yields between brackets.

https://dx.doi.org/10.1021/acs.energyfuels.0c02804
Energy Fuels XXXX, XXX, XXX−XXX

acidity per mass unit of coke produced were more noticeable in the case of catalyst ECAT-D than in catalyst ECAT-R. Once again, this behavior suggests that, at the same degree of conversion, catalyst ECAT-R is less affected by the coke deposition in comparison to catalyst ECAT-D, which contains a higher proportion of strong acidic sites, inducing a stronger adsorption of coke precursors and coke itself.

Brönsted and Lewis acid sites in the catalysts may interact differently with coke precursors and the end coke product. Table 8 shows how the different acid sites, both in quality and strength according to FTIR and pyridine TPD evidence, remain distributed in the coked catalysts after cracking of the various feedstocks, as compared to the fresh catalysts. It can be observed that, independently from the feedstock, coke formed on the catalysts impacts more severely on the Brönsted sites than on Lewis sites, particularly in the cases of the fractions that yield more coke, that is, AF and RF. Thus, it is to be expected that Brönsted sites will be more sensitive to coke forming processes. Moreover, it had also been postulated that Lewis sites in Y zeolites are more hidden in the structure,[63] a proposition that could justify the more important decrease in Brönsted sites after reaction.[20] In relation to the acid strength, it is clear that the stronger sites, which are more prone to adsorb coke precursors, are more severely affected, particularly in catalyst ECAT-D, which has a higher proportion of stronger sites when fresh. This severe effect on strong acidic sites was consistent with the increasing basic character of the feedstocks,[12,13] which followed the order SF < VGO < AF < RF.

Table 8. Percentage of Acid Sites in Catalysts Remaining after the Conversion of the Various Fractions at 500 °C[a]

	type of sites (%)				acid strength (%)			
	ECAT-D		ECAT-R		ECAT-D		ECAT-R	
feedstock	B	L	B	L	weak	strong	weak	strong
fresh	47	53	66	34	25	75	42	58
VGO	37	61	39	61	63	37	67	33
SF	42	58	46	54	59	41	59	41
AF	24	76	36	64	68	32	71	29
RF	15	85	30	70	73	27	74	26

[a]Site types according to FTIR, acid strength according to pyridine TPD. Conversion approximately 20 wt %.

CONCLUSIONS

The order of reactivity of a paraffinic VGO and its saturated (SF), aromatic (AF), and resin (RF) fractions over an octane-barrel and a resid type equilibrium FCC catalysts was SF > VGO > AF > RF. The conversion of the parent feedstock and the product yields cannot be reconstructed additively from the conversions of its individual fractions due to the interactions between components of the fractions when present in the VGO.

Given the individual compositions, the AF and RF fractions (with a high proportion of molecules having condensed aromatic rings with side chains, which could be easily dealkylated to aliphatic and aromatic hydrocarbons in the boiling range of gasoline) yielded significantly more gasoline than the SF fraction, which, in turn, showed the highest yield of LPG. Consistently, they produced much more aromatic compounds in the gasoline cut; oppositely, the SF fraction, with a high proportion of linear paraffins, yielded the highest proportion of paraffinic and olefinic hydrocarbons in the gasoline. Gasoline from the parent VGO had a similar result to that of the SF fraction, given its predominance in the parent feedstock.

The octane-barrel type catalyst ECAT-D, due to its higher and stronger acidity, was in general more active than the resid type catalyst ECAT-R. Nevertheless, the conversion of the highly polar resin fraction, including bulky molecules, was slightly higher over the catalyst ECAT-R, given the higher accessibility provided by mesopores. In general, for a given feedstock, the most active catalyst ECAT-D yielded more light products and coke than did catalyst ECAT-R. As expected, the quality of gasoline from the octane-barrel type catalyst (ECAT-D) was always better than that from catalyst ECAT-R.

The RF and AF fractions, which include coke precursors with a high molecular weight and basicity, which strongly adsorb on the acidic sites, produced more coke than the SF fraction, with the VGO showing an intermediate yield. Coke impacted more severely on Brönsted acid sites than on Lewis sites, particularly when the AF and RF fractions were cracked. The stronger sites were more severely affected by coke, particularly in catalyst ECAT-D, which has a higher amount of strong sites when fresh. This negative effect was consistent with the increasing basic character and coke forming trend of the feedstocks, following the order SF < VGO < AF < RF. The specific total and micropore (zeolitic) surface areas and mean mesopore diameters of both catalysts were also affected negatively by coke in the same order. Overall, the textural and acidic properties in catalyst ECAT-R were less affected than those in catalyst ECAT-D, with the differences being more important when the RF and AF fractions were cracked. Given the higher and stronger acidity of catalyst ECAT-D, which induces a stronger adsorption of coke intermediates and coke itself, coke on this catalyst was more condensed than that on catalyst ECAT-R.

This type of laboratory reactor and experiments soundly contributes to knowing the impact of a certain feedstock on FCC operation.

AUTHOR INFORMATION

Corresponding Author

Ulises Sedran − *Instituto de Investigaciones en Catálisis y Petroquímica "Ing. José Miguel Parera" INCAPE (UNL − CONICET), 3000 Santa Fe, Argentina;* orcid.org/0000-0002-4145-2834; Phone: +54 (342) 451-1370 #6102; Email: usedran@fiq.unl.edu.ar

Authors

Jayson Fals − *Instituto de Investigaciones en Catálisis y Petroquímica "Ing. José Miguel Parera" INCAPE (UNL − CONICET), 3000 Santa Fe, Argentina; Grupo de Investigación en Oxi/Hidro-Tratamiento Catalítico y Nuevos Materiales, Universidad del Atlántico, 081001 Puerto Colombia, Atlántico, Colombia*

Juan Rafael García − *Instituto de Investigaciones en Catálisis y Petroquímica "Ing. José Miguel Parera" INCAPE (UNL − CONICET), 3000 Santa Fe, Argentina;* orcid.org/0000-0002-6804-032X

Marisa Falco − *Instituto de Investigaciones en Catálisis y Petroquímica "Ing. José Miguel Parera" INCAPE (UNL − CONICET), 3000 Santa Fe, Argentina;* orcid.org/0000-0002-8410-6632

Complete contact information is available at:

https://dx.doi.org/10.1021/acs.energyfuels.0c02804
Energy Fuels XXXX, XXX, XXX−XXX

https://pubs.acs.org/10.1021/acs.energyfuels.0c02804

Notes

The authors declare no competing financial interest.

■ ACKNOWLEDGMENTS

This work was carried out with financial support of the University of Litoral (UNL, Santa Fe, Argentina), Secretary of Science and Technology, Proj. CAID 50420150100068LI, and the National Agency for Scientific and Technological Promotion (ANPCyT), PICT 1208/2016.

■ REFERENCES

(1) Xu, C.; Gao, J.; Zhao, S.; Lin, S. Correlation between feedstock SARA components and FCC product yields. *Fuel* **2005**, *84*, 669−674.
(2) Speight, J. *The Chemistry and Technology of Petroleum*, Fifth ed.; CRC Press-Taylor & Francis Group: Boca Raton, LA, 2014.
(3) Mendes, F. L.; Texeira da Silva, V.; Pacheco, M. E.; de Rezende Pinho, A.; Henriques, C. A. Hydrotreating of fast pyrolysis oil: A comparison of carbons and carboncovered alumina as supports for Ni2P. *Fuel* **2020**, *264*, 116764.
(4) Jiménez-García, G.; Aguilar-López, R.; Maya-Yescas, R. The fluidized-bed catalytic cracking unit building its future environment. *Fuel* **2011**, *90*, 3531−3541.
(5) Palos, R.; Gutierrez, A.; Fernández, M. L.; Trueba, D.; Bilbao, J.; Arandes, J. M. Upgrading of heavy coker naphtha by means of catalytic cracking in refinery FCC unit. *Fuel Process. Technol.* **2020**, *205*, 106454.
(6) Jiménez-García, G.; de Lasa, H.; Maya-Yescas, R. Simultaneous estimation of kinetics and catalysts activity during cracking of 1,3,5-tri-isopropyl benzene on FCC catalyst. *Catal. Today* **2014**, *220-222*, 178.
(7) Matheus, C. R. V.; Aguiar, E. F. S. The role of MPV reaction in the synthesis of propene from ethanol through the acetone route. *Catal. Commun.* **2020**, *145*, 106096.
(8) *Chemical Reactor Technology for Environmentally Safe Reactors and Products*; de Lasa, H., Dogu, G., Ravella, A. Eds.; Kluwer, Academic Publishers: Dordrecht, The Netherlands, 1992; Vol. *225*.
(9) Sadeghbeigi, R., *Fluid Catalytic Cracking Handbook*, Third ed.; Elsevier, 2012.
(10) Gilbert, W.; Morgado, E.; de Abreu, M.; de la Puente, G.; Passamonti, F.; Sedran, U. A novel fluid catalytic cracking approach for producing low aromatic LCO. *Fuel Process. Technol.* **2011**, *92*, 2235−2240.
(11) Al-Absi, A.; Aitani, A.; Al-Khattaf, S. Thermal and catalytic cracking of whole crude oils at high severity. *J. Anal. Appl. Pyrolysis* **2020**, *145*, 104705.
(12) Lappas, A.; Patiaka, D.; Dimitriadis, B.; Vasalos, I. Separation characterization and catalytic cracking kinetics of aromatic fractions obtained from FCC feedstocks. *Appl. Catal., A* **1997**, *152*, 7−26.
(13) Sanchez-Minero, F.; Ancheyta, J.; Silva-Oliver, G.; Flores-Valle, S. Predicting SARA composition of crude oil by means of NMR. *Fuel* **2013**, *110*, 318−321.
(14) Fan, T.; Buckley, J. Rapid and accurate SARA analysis of medium gravity crude oils. *Energy Fuels* **2002**, *16*, 1571−1575.
(15) Florez, M.; Guerrero, J.; Cabanzo, R.; Mejía-Ospino, E. SARA analysis and Conradson carbon residue prediction of Colombian crude oils using PLSR and Raman spectroscopy. *J. Pet. Sci. Eng.* **2017**, *156*, 966−970.
(16) Sahu, R.; Song, B.; Im, J.; Jeon, Y.; Lee, C. A review of recent advances in catalytic hydrocracking of heavy residues. *J. Ind. Eng. Chem.* **2015**, *27*, 12−24.
(17) Petti, T.; Tomczak, Z.; Pereira, C.; Cheng, W. Investigation of nickel species on commercial FCC equilibrium catalysts-implications on catalyst performance and laboratory evaluation. *Appl. Catal., A* **1998**, *169*, 95−109.
(18) Yuxia, Z.; Quansheng, D.; Wei, L.; Liwen, T.; Jun, L. Studies of iron effects on FCC catalysts. *Fluid Catalytic Cracking VII Materials, Methods and Process Innovations*; Elsevier, 2007; Vol. *166*, pp 201−212.
(19) *ASTM D2007-11: Standard test method for characteristic groups in rubber extender and processing oils and other petroleum-derived oils by the clay-gel absorption chromatographic method*; ASTM International, 2016.
(20) Fals, J.; García, J. R.; Falco, M.; Sedran, U. Coke from SARA fractions in VGO. Impact on Y zeolite acidity and physical properties. *Fuel* **2018**, *225*, 26−34.
(21) Mullins, O.; Sheu, E.; Hammami, A.; Marshall, A. *Asphaltenes, heavy oils and petroleomics*; Springer: New York, NY, 2007.
(22) Nalwaya, V.; Tantayakom, V.; Piumsomboon, P.; Fogler, S. Studies on asphaltenes through analysis of polar fractions. *Ind. Eng. Chem. Res.* **1999**, *38*, 964−972.
(23) Pereira, J. C.; Lopez, I.; Salas, R.; Silva, F.; Fernandez, C.; Urbina, C.; Lopez, J. C. Resins: The molecules responsible for the stability/instability phenomena of asphaltenes. *Energy Fuels* **2007**, *21*, 1317−1321.
(24) Al-Khattaf, S.; de Lasa, H. The role of diffusion in alkyl-benzenes catalytic cracking. *Appl. Catal., A* **2002**, *226*, 139−153.
(25) Scherzer, J. Octane-enhancing, zeolitic FCC catalysts: scientific and technical aspects. *Catal. Rev.: Sci. Eng.* **1989**, *31*, 215−354.
(26) Karakhanov, E.; Glotov, A.; Nikiforova, A.; Vutolkina, A.; Ivanov, A.; Kardashev, S.; Maksimov, A.; Lysenko, S. Catalytic cracking additives based on mesoporous MCM-41 for sulfur removal. *Fuel Process. Technol.* **2016**, *153*, 50−57.
(27) Bobkova, T.; Potapenko, O.; Doronin, V.; Sorokina, T. Transformations of n-undecane−indole model mixtures over the cracking catalysts resistant to nitrogen compounds. *Fuel Process. Technol.* **2018**, *172*, 172−178.
(28) Glotov, A.; Levshakov, N.; Vutolkina, A.; Lysenko, S.; Karakhanov, E.; Vinokurov, V. Aluminosilicates supported La-containing sulfur reduction additives for FCC catalyst: Correlation between activity, support structure and acidity. *Catal. Today* **2019**, *329*, 135−141.
(29) Pujro, R.; Falco, M.; Devard, A.; Sedran, U. Reactivity of the saturated, aromatic, and resin fractions of ATR resids under FCC conditions. *Fuel* **2014**, *119*, 219−225.
(30) Martinez, C.; Verboekend, D.; Pérez-Ramírez, J.; Corma, A. Stabilized hierarchical USY zeolite catalysts for simultaneous increase in diesel and LPG olefinicity during catalytic cracking. *Catal. Sci. Technol.* **2013**, *3*, 972−981.
(31) García, J. R.; Falco, M.; Sedran, U. Impact of the desilication treatment of Y zeolite on the catalytic cracking of bulky hydrocarbon molecules. *Top. Catal.* **2016**, *59*, 268−277.
(32) Wojciechowski, B.; Corma, A. Catalytic Cracking: Catalysts. *Chemistry, and Kinetics*; Marcel Dekker: New York, NY, 1986.
(33) Guisnet, M.; Magnoux, P. Organic chemistry of coke formation. *Appl. Catal., A* **2001**, *212*, 83−96.
(34) Ochoa, A.; Vicente, H.; Sierra, I.; Arandes, J. M.; Castaño, P. Implications of feeding or cofeeding bio-oil in the fluid catalytic cracker (FCC) in terms of regeneration kinetics and energy balance. *Energy* **2020**, *209*, 118467.
(35) Cerqueira, H.; Caeiro, G.; Costa, L.; Ribeiro, F. R. Deactivation of FCC catalysts. *J. Mol. Catal. A: Chem.* **2008**, *292*, 1−13.
(36) Guisnet, M.; Costa, L.; Ribeiro, F. R. Prevention of zeolite deactivation by coking. *J. Mol. Catal. A: Chem.* **2009**, *305*, 69−83.
(37) Ibarra, A.; Veloso, A.; Bilbao, J.; Arandes, J.; Castaño, P. Dual coke deactivation pathways during the catalytic cracking of raw bio-oil and vacuum gasoil in FCC conditions. *Appl. Catal., B* **2016**, *182*, 336−346.
(38) Passamonti, F. J.; Puente, G. d. l.; Sedran, U. Comparison between MAT flow fixed bed and batch fluidized bed reactors in the evaluation of FCC catalysts. 1. Conversion and yields of the main hydrocarbon groups. *Energy Fuels* **2009**, *23*, 1358−1363.
(39) Sanchez-Castillo, M. A.; Madon, R. J.; Dumesic, J. A. Role of rare earth cations in Y zeolite for hydrocarbon cracking. *J. Phys. Chem. B* **2005**, *109*, 2164−2175.

https://dx.doi.org/10.1021/acs.energyfuels.0c02804
Energy Fuels XXXX, XXX, XXX−XXX

(40) Trigueiro, F.; Monteiro, D.; Zotin, F.; Sousa-Aguiar, E. F. Thermal stability of Y zeolites containing different rare earth cations. *J. Alloys Compd.* **2002**, *344*, 337−341.
(41) Pekediz, A.; Kraemer, D.; Chabot, J.; de Lasa, H. Mixing Patterns in a Novel Riser Simulator. In *Chemical Reactor Technology for Environmentally Safe Reactors and Products*; de Lasa, H., Dogu, G., Ravella, A., Eds.; Kluwer, Academic Publishers: Dordrecht, The Netherlands, 1992; Vol. *225*, pp 133−146.
(42) Anderson, P.; Sharkey, J.; Walsh, R. Calculation of the research octane number of motor gasolines from gas chromatographic data and a new approach to motor gasoline quality control. *J. Inst. Petr.* **1972**, *58*, 83−94.
(43) Johnson, M. F. L. Estimation of the zeolite content of a catalyst from nitrogen adsorption isotherms. *J. Catal.* **1978**, *52*, 425−431.
(44) Emeis, C. Determination of integrated molar extinction coefficients for infrared absorption bands of pyridine adsorbed on solid acid catalysts. *J. Catal.* **1993**, *141*, 347−54.
(45) Aguayo, A.; Castaño, P.; Mier, D.; Gayubo, A.; Olazar, M.; Bilbao, J. Effect of cofeeding butane with methanol on the deactivation by coke of a HZSM-5 zeolite catalyst. *Ind. Eng. Chem. Res.* **2011**, *50*, 9980−9988.
(46) Castaño, P.; Elordi, G.; Olazar, M.; Bilbao, J. Imaging the profiles of deactivating species on the catalyst used for the cracking of waste polyethylene by combined microscopies. *ChemCatChem* **2012**, *4*, 631−635.
(47) Behera, B.; Ray, S.; Singh, I. Structural characterization of FCC feeds from Indian refineries by NMR spectroscopy. *Fuel* **2008**, *87*, 2322−2333.
(48) Bozzano, G.; Dente, M.; Carlucci, F. The effect of naphthenic components in the visbreaking modeling. *Comput. Chem. Eng.* **2005**, *29*, 1439−1446.
(49) Stratiev, D.; Shishkova, I.; Tsaneva, T.; Mitkova, M.; Yordanov, D. Investigation of relations between properties of vacuum residual oils from different origin, and of their deasphalted and asphaltene fractions. *Fuel* **2016**, *170*, 115−129.
(50) Ancheyta-Juarez, J.; Lopez-Isunza, F.; Aguilar-Rodriguez, E. Correlations for predicting the effect of feedstock properties on catalytic cracking kinetic parameters. *Ind. Eng. Chem. Res.* **1998**, *37*, 4637−4640.
(51) Nilsson, P.; Otterstedt, J. Effect of composition of the feedstock on the catalytic cracking of heavy vacuum gas oil. *Appl. Catal.* **1987**, *33*, 145−156.
(52) Gao, J.; Xu, C.; Lin, S.; Yang, G.; Guo, Y. Simulations of gas−liquid−solid 3-phase flow and reaction in FCC riser reactors. *AIChE J.* **2001**, *47*, 677−692.
(53) Passamonti, F.; de La Puente, G.; Gilbert, W.; Morgado, E.; Sedran, U. Comparison between fixed fluidized bed (FFB) and batch fluidized bed reactors in the evaluation of FCC catalysts. *Chem. Eng. J.* **2012**, *183*, 433−447.
(54) Meirer, F.; Kalirai, S.; Morris, D.; Soparawalla, S.; Liu, Y.; Mesu, G.; Andrews, J.; Weckhuysen, B. Life and death of a single catalytic cracking particle. *Sci. Adv.* **2015**, *1*, e1400199.
(55) Falco, M.; Morgado, E.; Amadeo, N.; Sedran, U. Accessibility in alumina matrices of FCC catalysts. *Appl. Catal., A* **2006**, *315*, 29−34.
(56) Garcia, J. R.; Bertero, M.; Falco, M.; Sedran, U. Catalytic cracking of bio-oils improved by the formation of mesopores by means of Y zeolite desilication. *Appl. Catal., A* **2015**, *503*, 1−8.
(57) Garcia, J. R.; Falco, M.; Sedran, U. Intracrystalline mesoporosity over Y zeolites: PASCA evaluation of the secondary cracking inhibition in the catalytic cracking of hydrocarbons. *Ind. Eng. Chem. Res.* **2017**, *56*, 1416−1423.
(58) Garcia, J. R.; Falco, M.; Sedran, U. Intracrystalline mesoporosity over Y zeolites. Processing of VGO and resid-VGO mixtures in FCC. *Catal. Today* **2017**, *296*, 247−253.
(59) Bertero, M.; Garcia, J. R.; Falco, M.; Sedran, U. Equilibrium FCC catalysts to improve liquid products from biomass pyrolysis. *Renewable Energy* **2019**, *132*, 11−18.
(60) Bertero, M.; Garcia, J. R.; Falco, M.; Sedran, U. Conversion of cow manure pyrolytic tar under FCC conditions over modified equilibrium catalysts. *Waste Biomass Valorization* **2020**, *11*, 2925−2933.
(61) Mochizuki, H.; Yokoi, T.; Imai, H.; Namba, S.; Kondo, J. N.; Tatsumi, T. Effect of desilication of H-ZSM-5 by alkali treatment on catalytic performance in hexane cracking. *Appl. Catal., A* **2012**, *449*, 188−197.
(62) Stratiev, D.; Galkin, V.; Shishkova, I.; Minkov, D.; Stanulov, K. Yield of products from catalytic cracking of vacuum gasoils. *Chem. Technol. Fuels Oils* **2007**, *43*, 311−318.
(63) Jacobs, P. A.; Martens, J. A. Chapter 12 introduction to acid catalysis with zeolites in hydrocarbon reactions. *Stud. Surf. Sci. Catal.* **1991**, *58*, 445−496.

https://dx.doi.org/10.1021/acs.energyfuels.0c02804
Energy Fuels XXXX, XXX, XXX−XXX